

Excitonic gap, phase transition, and quantum Hall effect in graphene: strong-coupling regime

V.P. Gusynin

Bogolyubov Institute for Theoretical Physics, 03143, Kiev, Ukraine

V.A. Miransky*

*Department of Applied Mathematics, University of Western Ontario, London, Ontario N6A 5B7, Canada
and Yukawa Institute for Theoretical Physics, Kyoto University, Kyoto 606-8502, Japan*

S.G. Sharapov

Department of Physics and Astronomy, McMaster University, Hamilton, Ontario L8S 4M1, Canada

I.A. Shovkovy*

Department of Physics, Western Illinois University, Macomb, IL 61455, USA

(Dated: November 8, 2018)

We suggest that physics underlying the recently observed removal of sublattice and spin degeneracies in graphene in a strong magnetic field describes a phase transition connected with the generation of excitonic and spin gaps. The strong-coupling regime is described using a phenomenological model with enhanced Zeeman splitting (spin gap) and excitonic gaps. The experimental form of the Hall conductivity σ_{xy} with the additional $\nu = 0, \pm 1$ plateaus is reproduced. The form of σ_{xy} in the case of a strong-coupling regime with no enhanced Zeeman splitting is also discussed.

PACS numbers: 73.43.Cd, 71.70.Di, 81.05.Uw

I. INTRODUCTION

In a recent paper Ref. 1, hereafter referred to as *I*, we considered how the new plateaus in the Hall conductivity of graphene discovered by Y. Zhang *et al.*² develop, assuming the weak-coupling regime of the magnetic catalysis scenario. We have become aware of the experiments³ showing that the $\nu = 0$ plateau in the Hall conductivity exists even at rather high temperatures. This fact indicates the relevance of a strong-coupling regime. It is the purpose of the present work to complete the theoretical analysis of *I* by considering also the strong-coupling regime.

A graphite monolayer, or *graphene*, has become a new exciting topic in physics of two dimensional electronic systems.^{4,5,6} A qualitatively new feature of graphene is that the eigenfunctions and the eigenvalues of the low energy quasiparticle excitations are described by the relativistic 2+1 dimensional Dirac theory. The spinor structure of the wave functions is a general consequence of the honeycomb lattice structure of graphene with two carbon atoms per unit cell.^{7,8} When a magnetic field is applied, noninteracting Dirac quasiparticles occupy Landau levels (LLs) with the energies

$$E_n = \text{sgn}(n) \sqrt{2|n|\hbar v_F^2 |eB|/c} \quad (1)$$

$$\approx 424 \text{sgn}(n) \sqrt{|n|} \sqrt{B[\text{T}]} \text{K}, \quad n = 0, \pm 1, \pm 2, \dots$$

Here to estimate the energies E_n , the value of the Fermi velocity $v_F = 10^6 \text{m/s}$ was used, and the magnetic field B orthogonal to the graphene's plane is given in Tesla. Several anomalous properties of graphene are attributed

to the presence in the spectrum (1) of the $n = 0$ field independent lowest Landau level (LLL). In the diagonal conductivity, the anomaly manifests itself as the phase shift of π of the quantum magnetic oscillations expected theoretically both using the semiclassical quantization condition for the quasiparticles with a linear dispersion⁹ and from a microscopical calculation valid both for the massless and massive Dirac fermions.^{10,11} Accordingly, in the Hall conductivity the anomaly results in the anomalous integer quantum Hall (QH) effect with the plateaus at the filling factors $\nu = \pm 4(|n| + 1/2)$.^{12,13,14,15} These theoretical conceptions allowed to identify unambiguously the Dirac quasiparticles in the two independent experiments.^{16,17} At present a lot of studies on graphene are concentrated on phenomena whose understanding demands going beyond unconventional but yet rather simple physics of noninteracting Dirac quasiparticles.

On the experimental side, for a magnetic field $B \gtrsim 20 \text{T}$, the appearance of additional QH plateaus with the filling factors $\nu = 0, \pm 1, \pm 4$ was reported in Ref. 2. The theoretical studies of these additional plateaus in graphene can be divided into four classes.

(i) Fractional QH effect. Although there is no experimental evidence for such an effect in graphene so far, there are a few theoretical papers, where this possibility is discussed.^{15,18,19,20}

The remaining three scenarios consider various possibilities of breaking the $U(4)$ symmetry of the noninteracting Hamiltonian of graphene. While this symmetry remains intact in the presence of a long-range Coulomb interaction and at a nonzero chemical potential μ , it is explicitly broken in the presence of the Zeeman and some types of short-range interactions.

(ii) A model with local (on-site) interactions which explicitly break the $U(4)$ symmetry was considered in Ref. 21.

(iii) An analogy between the four-fold degeneracy of LLs in graphene associated with the $U(4)$ symmetry and the $SU(4)$ ferromagnetism studied previously in the bilayer quantum Hall systems²² is exploited in Refs. 23,24. In this QH ferromagnetism scenario the QH plateaus with *all* integer values of the filling factor ν occur. The current experimental data,² however, do not seem to support the existence of the plateaus with $\nu = \pm 3, \pm 5, \dots$

(iv) The magnetic catalysis scenario was considered in *I* and in Refs. 25,26. It is based on the phenomenon of the electron-hole (fermion-antifermion) pairing in a magnetic field revealed in field theory²⁷ and the analysis in Refs. 28,29,30,31, where this phenomenon was considered in graphene. (This analysis was originally inspired by the early experiments in highly oriented pyrolytic graphite.³²) In Refs. 28,29,30,31, the spontaneous breakdown of the $U(4)$ symmetry by generating a dynamical excitonic gap Δ was considered. A new development for this scenario suggested in *I* was to fit the data of Ref. 2 by including both the Zeeman term and the excitonic gap. The central feature of this scenario is that the only plateaus in the Hall conductivity σ_{xy} are those with $\nu = 0, \pm 1$ and $\nu = \pm 2k$ ($k = 1, 2, \dots$), i.e., the plateaus observed in experiment.² While in *I* the excitonic gap is produced by the Coulomb interactions, local (on-site) interactions are used for this purpose in Ref. 25. A dynamics relating to the magnetic catalysis scenario was considered in Ref. 33, in which an excitoniclike gap is produced by electron-phonon interactions.

As was emphasized in *I*, while the plateau $\nu = 0$ could even appear either due to the spin splitting or the excitonic gap Δ alone, the plateaus $\nu = \pm 1$ arise only if both the spin splitting and the gap Δ are non-vanishing. In other words, the plateaus $\nu = \pm 1$ are generated by the dynamics which completely removes the $U(4)$ degeneracy of the LLL. This can for example be seen explicitly from the expression for the Hall conductivity due to the $n = 0$ Landau level in the clean limit (i.e., in the limit of the vanishing scattering rate of quasiparticles):

$$\sigma_{xy} = -\frac{e^2}{h} \text{sgn}(eB) \times [\text{sgn}(\mu_+) \theta(|\mu_+| - \Delta) + \text{sgn}(\mu_-) \theta(|\mu_-| - \Delta)], \quad (2)$$

where $\mu_{\pm} = \mu \pm E_Z$ with E_Z being the Zeeman energy. The fitting procedure in *I* is heavily based on the assumption that the Zeeman energy is

$$E_Z = \frac{g_L}{2} \mu_B B \simeq 0.67 B[\text{T}] \text{ K}, \quad (3)$$

where $\mu_B = e\hbar/(2mc)$ is the Bohr magneton and the Lande factor in graphene is $g_L \simeq 2$. For typical strengths of the magnetic field used in the experiment, $B \lesssim 45 \text{ T}$, the Zeeman energy (3) is $E_Z \lesssim 30 \text{ K}$. By combining this observation with the fact that the $\nu = 0$ and $\nu = \pm 1$

plateaus have comparable widths,² it was concluded that the excitonic gap Δ is of the same order as E_Z . Indeed, as seen from Eq. (2), it is the interplay between these two energy scales, Δ and E_Z , that determines the size of the lowest plateaus. The required magnitude (of several dozens of Kelvin) for the excitonic gap corresponds to the weak-coupling regime. In *I*, the best fit was found at $g = e^2/(\epsilon\hbar v_F) \simeq 0.07$, where ϵ is the dielectric constant of the medium. An immediate implication of such a weakly coupled dynamics is that the typical magnitude of the critical temperature, at which the gap disappears, is of the same order of a dozen of Kelvin.

In part, the motivation for the present work is the new experimental data³ suggesting that the $\nu = 0$ plateau, observed for strong magnetic fields, may persist even at rather high temperatures. This alone would suggest the relevance of the strong-coupling regime with $g \gtrsim 1$. Moreover, as will be shown in Sec. II in detail, this regime is also consistent with the structure of the higher plateaus in the Hall conductivity reported in Ref. 2.

In contrast to the weak-coupling regime, the dynamics at strong coupling is non-perturbative and, therefore, permits no rigorous quantitative analysis. In addition, the simple type of the dynamics discussed in *I* is not sufficient to fit the experimental data in Ref. 2. This is because of a very large hierarchy between the energy scales set by the Zeeman splitting (3) and the excitonic gap at strong coupling. In a consistent approach, as will be discussed below, an anomalous enhancement of the Zeeman-like splitting will be required.

Because of the difficulties due to the non-perturbative dynamics at strong coupling, we use a phenomenological approach in this paper. Therefore, most conclusions of the analysis below should be viewed only as qualitative. As we shall see, however, many of them are likely to be very robust. For example, the critical temperature for the excitonic condensate as well as for the related appearance of the plateaus $\nu = 0, \pm 1$ should be of the same order as the excitonic gap, i.e., a few hundred Kelvin.

The paper is organized as follows. In Sec. II, we analyze the experimental data of Ref. 2 in detail, and extract the constraints on the dynamics to be implemented in a phenomenological model. The model itself is introduced in Sec. III. In Sec. IV, we present a fit of the experimental data for the $\nu = 0, \pm 1$ as well as the higher plateaus, and underline the specific features of the strong-coupling regime. In Sec. V, for completeness and better understanding the role of the Zeeman splitting, we consider the dynamics in the strong-coupling regime with no enhanced Zeeman splitting. In this case, besides the standard sequence $\nu = (4n + 2)$, the only additional plateau is that with $\nu = 0$. In Sec. VI, the main results of the paper are summarized.

II. ANALYSIS OF THE EXPERIMENTAL DATA

The low-energy quasiparticle excitations in graphene are described in terms of a four-component Dirac spinor $\Psi_\sigma^T = (\psi_{KA\sigma}, \psi_{KB\sigma}, \psi_{K'B\sigma}, \psi_{K'A\sigma})$. This spinor combines the Bloch states with spin $\sigma = \pm 1$ on the two different sublattices (A, B) of the hexagonal graphene lattice and with momenta near the two inequivalent points (K, K') at the opposite corners of the two-dimensional Brillouin zone.

The free, low-energy quasiparticle Hamiltonian for zero carrier density (or $\mu = 0$) and in absence of the Zeeman splitting can be recast in a relativistic form,

$$H_0 = -iv_F \int d^2\mathbf{r} \bar{\Psi}_\sigma (\gamma^1 \hbar \nabla_x + \gamma^2 \hbar \nabla_y) \Psi_\sigma, \quad (4)$$

where $\bar{\Psi}_\sigma = \Psi_\sigma^\dagger \gamma^0$ is the Dirac conjugated spinor and summation over spin σ is understood. Notice that the Fermi velocity $v_F \approx 10^6$ m/s plays the role of the speed of light. In Eq. (4), γ^ν , $\nu = 0, 1, 2$, are 4×4 gamma matrices belonging to a reducible representation of the Dirac algebra: $\gamma^\nu = \tilde{\tau}_3 \otimes (\tau_3, i\tau_2, -i\tau_1)$, where the Pauli matrices $\tilde{\tau}, \tau$ act in the subspaces of the valley (K, K') and sublattices (A, B) indices, respectively. The matrices satisfy the usual anticommutation relations $\{\gamma^\mu, \gamma^\nu\} = 2g^{\mu\nu}$, $g^{\mu\nu} = (1, -1, -1)$, $\mu, \nu = 0, 1, 2$. The orbital effect of a magnetic field \mathbf{B} applied perpendicular to the graphene plane is included via the covariant derivative $\nabla = \partial + (ie/\hbar c)\mathbf{A}$.

The explicit form of the interaction Hamiltonian and the effective action are derived and discussed in I. We describe their features in the strong-coupling regime below.

A. Relationship between the gate voltage and μ

In experiments^{2,4,16,17} the density of carriers (or carrier imbalance ρ which is the difference between the densities of electron and holes) is tunable by the gate voltage V_g applied to the Si substrate of a graphene device. The measurements of the Hall coefficient and a (consistent with them) theoretical estimate give the relationship¹⁶

$$\rho = \alpha(V_g - V_0), \quad \alpha \approx 7.3 \times 10^{10} \text{ cm}^{-2} \text{ V}^{-1}, \quad (5)$$

where the shift V_0 is attributed to the shift of the Dirac point due to an unintentional doping.⁴ In our analysis of the experimental data,² the value of the shift is in the range from 0.8 V to 5.8 V.

On the theory side, the variation of the density of carriers in the system is modeled through adding to the Hamiltonian (4) the term $-\mu \bar{\Psi}_\sigma \gamma^0 \Psi_\sigma = -\mu \Psi_\sigma^\dagger \Psi_\sigma$ with a tunable chemical potential μ . In order to make a connection between the experiment and the theory, one needs to know the relationship between the chemical potential μ and the carrier imbalance ρ .

We have examined the data of Ref. 2 relying on the following two natural *assumptions*:

- (i) the middle point of a step between two neighboring plateaus is associated with the value of the chemical potential in the middle of a smeared Landau level, and
- (ii) the middle of a plateau is associated with the value of the chemical potential in the middle of the energy gap between two Landau (sub)-levels.

The meaning of these two assumptions might be easier to grasp by referring to the correspondence between the quasiparticle energy spectrum and the structure of the Hall conductivity plateaus as shown, e.g., in Fig. 5 below.

We note that the structure of the higher plateaus can be used to extract the dependence $\mu(V_g)$. In the corresponding analysis it is useful to assume that only the plateaus $\nu = 0, \pm 1, \pm 2$ (connected with the LLL) are affected by the excitonic gap. This qualitative feature is a rigorous outcome in the weak-coupling regime of I. If it holds also at strong coupling, which is at least plausible,²⁷ the dynamics of the exciton condensation would not contaminate the structure of the higher plateaus in the Hall conductivity. Then, for the filling factors $\nu = \pm 3, \pm 4, \pm 5$, one derives the following relations:

$$V_g(\nu = \pm 4) = V_g(\mu = E_{\pm 1}), \quad (6a)$$

$$V_g(\nu = \pm 3) = V_g(\mu = E_{\pm 1} \mp E_Z), \quad (6b)$$

$$V_g(\nu = \pm 5) = V_g(\mu = E_{\pm 1} \pm E_Z), \quad (6c)$$

where Eqs. (6b), (6c), and Eq. (6a) are based on the assumptions (i) and (ii), respectively [see also Fig. 5 below]. In the analysis it is reasonable to accept that the Zeeman-like energy E_Z , characterizing the Landau level splitting, is considerably smaller than E_1 (i.e., $E_Z \ll E_1$) even if E_Z is substantially enhanced compared to the ordinary Zeeman energy in Eq. (3). As we will see in Subsec. IIB and IIC below, this hierarchy of scales is indeed consistent with the strong-coupling regime: while $E_Z \simeq 100$ K, the energy $E_1 \simeq 1000$ K. The results of the analysis are summarized in Figs. 1 and 2.

In Fig. 1, the experimental data for three specific combinations of the gate voltage differences are plotted as functions of the external magnetic field. After taking into account the correspondence between the filling factors and the values of the chemical potential in Eq. (6), we see that all three gate voltage differences,

$$\frac{1}{2} [V_g(\nu = 4) - V_g(\nu = -4)], \quad (7a)$$

$$\frac{1}{2} [V_g(\nu = 5) - V_g(\nu = -3)], \quad (7b)$$

$$\frac{1}{2} [V_g(\nu = 3) - V_g(\nu = -5)], \quad (7c)$$

determine the average value of the voltage (measured from V_0) that, up to higher order corrections, corresponds to $\mu = E_1$, i.e., $\mu = 424\sqrt{B} [\text{T}] \text{ K}$, see Eq. (1). (Note that to linear order the corrections due to Zeeman splitting cancel in all three combinations.) From Fig. 1, we

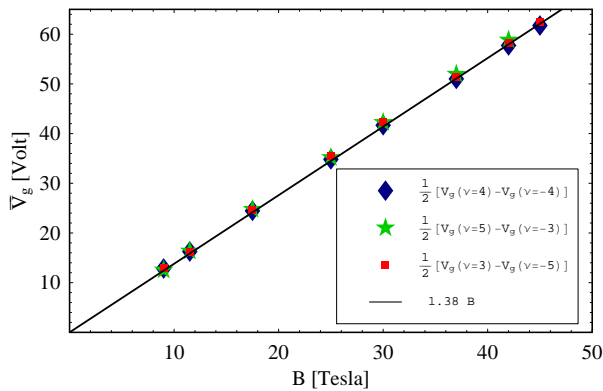


FIG. 1: (Color online) The compilation of the experimental data from Ref. 2 for the gate voltage $V_g(\nu)$ differences, $1/2[V_g(\nu = 4) - V_g(\nu = -4)]$, $1/2[V_g(\nu = 5) - V_g(\nu = -3)]$ and $1/2[V_g(\nu = 3) - V_g(\nu = -5)]$ as a function of the magnetic field B .

see that the dependence of the voltage on the magnetic field is described almost perfectly by the following linear fit: $\bar{V}_g(B) \approx 1.38 B[\text{T}] \text{ V}$ where $\bar{V}_g \equiv |V_g - V_0|$ and V_0 describes the shift of the Dirac point, see Eq. (5). Therefore, by trading the magnetic field B for the corresponding chemical potential, i.e., $\mu = 424\sqrt{B}[\text{T}] \text{ K}$, we get

$$\bar{V}_g \approx \left(\frac{\mu[\text{K}]}{361} \right)^2 \text{ V.} \quad (8)$$

By inverting this relation, we arrive at the following one:

$$\mu = \kappa \text{sgn}(V_g - V_0) \sqrt{|V_g - V_0|}, \quad \kappa \approx 361 \text{ K V}^{-1/2}. \quad (9)$$

The relations (8) and (9) will be used below to make a contact between the theory and the experiment. [The relation (9) is shown in Fig. 5 below by a dotted line.]

Another independent derivation of the relationship between V_g and μ can be obtained by fitting a sequence of several Landau levels E_n at a fixed value of the magnetic field. In Ref. 2, several lowest plateaus that correspond to the filling factors $\nu = 4n$ (with an integer n) were observed for the four lowest values of the field. In accordance with our assumption (ii), the corresponding values of the voltage are associated with the chemical potentials in the middle of the energy gap between the two sublevels of the Zeeman-split n th Landau level, i.e., $\mu = E_n$ to linear order. By making use of Eq. (1), the corresponding chemical potentials are given by $\mu = 212 \text{sgn}(\nu) \sqrt{|\nu B|}[\text{T}] \text{ K}$ with $\nu = 4n$.

The experimental data for the voltage differences that correspond to the first few observed sets of the filling factors are plotted versus νB in Fig. 2. This dependence is well approximated by a linear function, $\bar{V}_g \approx (1.05 + 0.33 \nu B [\text{T}]) \text{ V}$. Note that because of limited data for low B , the value 1.05 V of a small intercept term

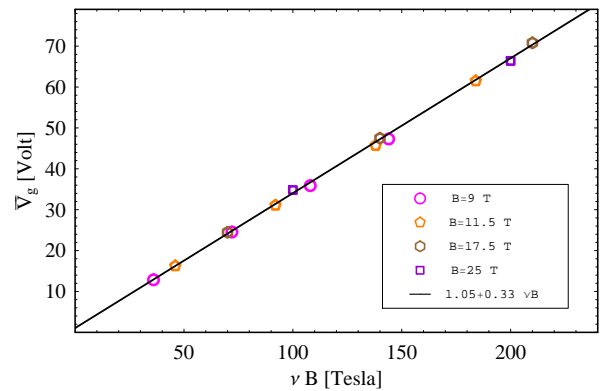


FIG. 2: (Color online) The compilation of the experimental data from Ref. 2 for the voltage differences $1/2[V_g(\sqrt{|\nu/2|\hbar v_F^2|eB|/c}) - V_g(-\sqrt{|\nu/2|\hbar v_F^2|eB|/c})]$ that correspond to the first few observed sets of the filling factors as a function of νB for four values of the field $B = 9, 11.5, 17.5, 25 \text{ T}$.

$\lesssim V_0$ is not reliable and will be omitted. Then, by expressing νB in terms of the chemical potential (as discussed in the previous paragraph), we arrive at the relation $\bar{V}_g \approx (\mu[\text{K}]/369)^2 \text{ V}$, which agrees reasonably well with Eq. (8).

Interestingly, the relation (9) with practically the same coefficient κ also follows from the equation $\mu^2 = \pi \hbar^2 v_F^2 |\rho|$ for the ideal gas of Dirac quasiparticles at $T = B = 0$ used in Refs. 14,29. Note however that the simultaneous use of Eq. (9) and the usual (i.e., without enhancement) Zeeman splitting (3) would lead to inconsistencies in fitting the experimental data. This was the reason for considering another relation between μ and V_g at weak-coupling in *I*.

B. Zeeman term

Now we are in a position to discuss the second, Zeeman term $\mu_B B \bar{\Psi} \gamma^0 \sigma_3 \Psi = \mu_B B \Psi^\dagger \sigma_3 \Psi$ which has to be added to the free Hamiltonian (4) (here the σ_3 matrix acts on spin indices). Considering the weak-coupling regime in *I*, we assumed that the Zeeman splitting is usual as given by Eq. (3). There are, however, theoretical arguments^{23,24,34} that the Coulomb interaction in the exchange channel may strongly enhance Zeeman splitting and lead to a spin gap Δ_Z (expressed through the condensate $(\bar{\Psi} \gamma^0 \sigma_3 \Psi)$) as large as a few hundred Kelvin.

Using the experimental data of Ref. 2, the energy of the Zeeman splitting can be found from the size of $\nu = \pm 4$ plateau whose appearance is attributed to the lifting of the spin degeneracy of the $n = \pm 1$ Landau level. We estimate the size of this plateau by extracting the following gate voltage differences: $\delta V_g \equiv 1/2[V_g(\mu = E_1 + E_Z) - V_g(\mu = E_1 - E_Z)] \approx 1/2[V_g(\mu = E_{-1} + E_Z) - V_g(\mu = E_{-1} - E_Z)]$. The results are presented in Fig. 3. We find

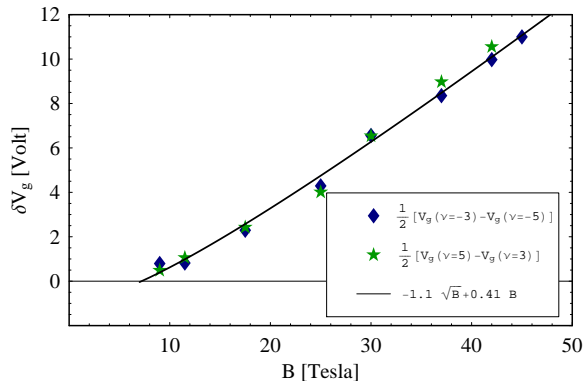


FIG. 3: (Color online) The compilation of the experimental data from Ref. 2 for the size of the $\nu = 4$ plateau that determines the Zeeman splitting of the first Landau level.

that the size of $\sigma_{xy} = \pm 4e^2/h$ plateau is reasonably well fitted by the dependence

$$\delta V_g(B) \approx (-1.1\sqrt{B[\text{T}]} + 0.41B[\text{T}]) \text{ V} \quad (10)$$

for $9 \text{ T} < B < 45 \text{ T}$. On the other hand, if $\delta\mu$, corresponding to δV_g , is reasonably small, one can differentiate expression (8) to obtain the relation $\delta V_g \approx 2\mu[\text{K}] \delta\mu[\text{K}]/(361)^2 \text{ V}$ (here the differentials dV_g and $d\mu$ were replaced by δV_g and $\delta\mu$, respectively). Now, substituting the chemical potential $\mu = E_1 = 424\sqrt{B[\text{T}]} \text{ K}$ and the splitting $\delta\mu = E_Z$ in this expression for δV_g and comparing it with Eq. (10), we arrive at the relation

$$E_Z = (63\sqrt{B[\text{T}]} - 169) \text{ K}. \quad (11)$$

This is 3 to 8 times larger than the usual Zeeman energy (3) for $9 \text{ T} < B < 45 \text{ T}$, providing another argument in favor of strong coupling. The large difference between the enhanced Zeeman energy(11) and conventional Zeeman energy (3) is likely caused by dynamical effects.^{23,24,34} In general, these effects should be sensitive to the temperature and chemical potential, so that E_Z is also a function of T and μ . Here, however, we restrict ourselves by the dependence E_Z on B .

C. Gap terms and the $\nu = \pm 1$ plateaus

As is clear from Eq. (2), the $\nu = \pm 1$ plateaus of the Hall conductivity observed in Ref. 2 can exist only if there is Zeeman splitting *and* the spectrum (1) is gapped, viz.

$$E_n = \text{sgn}(n)\sqrt{2|n|\hbar v_F^2|eB|/c + \Delta^2}. \quad (12)$$

In this case the four-fold degeneracy of the LLL ($n = 0$) is completely lifted.

Considering the dependence of σ_{xy} on μ in Eq. (2), one can see that while the size of the $\nu = \pm 1$ plateaus is $\delta\mu_1 \simeq$

$2E_Z$, the size of the 0th plateau is $\delta\mu_0 \simeq 2(\Delta - E_Z)$. The experiment in Ref. 2 measures the dependence $\sigma_{xy}(V_g)$ and indicates that the sizes of the 0th and $\nu = \pm 1$ plateaus (as a function of V_g) are comparable. Using Eq. (9), we estimate the V_g -size of the $\nu = \pm 1$ plateaus as $4\Delta E_Z/\kappa^2$ (in Volts), while the size of the 0th plateau is $2(\Delta - E_Z)^2/\kappa^2$ (in Volts). By simply requiring these two quantities to be equal, we derive $\Delta \simeq (2 + \sqrt{3})E_Z$. By making use of the Zeeman energy (11) extracted from experiment, we obtain $E_Z \approx 176 \text{ K}$ at a moderately strong field $B = 30 \text{ T}$. Therefore, a typical value of the excitonic gap is $\Delta \simeq 657 \text{ K}$.

It was assumed in *I* that the gap Δ in Eq. (12) is driven by the singlet excitonic order parameter

$$\begin{aligned} \langle \overline{\Psi} \sigma_0 \Psi \rangle = & \sum_{\sigma=\pm 1} \langle [\psi_{KA\sigma}^\dagger \psi_{KA\sigma} + \psi_{K'A\sigma}^\dagger \psi_{K'A\sigma} \\ & - \psi_{KB\sigma}^\dagger \psi_{KB\sigma} - \psi_{K'B\sigma}^\dagger \psi_{K'B\sigma}] \rangle, \end{aligned} \quad (13)$$

where we explicitly wrote unit matrix σ_0 acting on spin indices to underline the singlet character of this order parameter. The Zeeman interaction, however, may favor^{25,31} the triplet order parameter, $\langle \overline{\Psi} \boldsymbol{\sigma} \Psi \rangle$, where the vector $\boldsymbol{\sigma} = (\sigma_1, \sigma_2, \sigma_3)$ made from Pauli matrices acting on spin indices. Therefore, in addition to the singlet order parameter (13), one may also include the triplet order parameter³⁵

$$\begin{aligned} \langle \overline{\Psi} \boldsymbol{\sigma} \Psi \rangle = & \sum_{\sigma=\pm 1} \sigma \langle [\psi_{KA\sigma}^\dagger \psi_{KA\sigma} + \psi_{K'A\sigma}^\dagger \psi_{K'A\sigma} \\ & - \psi_{KB\sigma}^\dagger \psi_{KB\sigma} - \psi_{K'B\sigma}^\dagger \psi_{K'B\sigma}] \rangle. \end{aligned} \quad (14)$$

In the language of symmetry, the Zeeman term explicitly breaks the $U(4)$ symmetry down to the $U(2)_c \times U(2)_d$ (see Appendix C of *I*). [Note that the condensates $\langle \overline{\Psi} \sigma_1 \Psi \rangle$ and $\langle \overline{\Psi} \sigma_2 \Psi \rangle$ would spontaneously break the $SO(2)$ symmetry of the in-plane rotations and will not be considered here.] The dynamical generation of the gaps connected with order parameters (13) and (14) leads to the spontaneous breakdown of the $U(2)_c \times U(2)_d$ symmetry down to the abelian $U(1)_1 \times U(1)_2 \times U(1)_3 \times U(1)_4$ one. There might exist also other gaps that break the $U(2)_c \times U(2)_d$ symmetry. Therefore, the problem is very complicated in general due to the potential possibility of many competing order parameters.

III. PHENOMENOLOGICAL MODEL

There are several ways to tackle the problem of competing order parameters in graphene. The best way would be to include all relevant interactions and study the instability of the system with respect to the formation of all possible condensates. An approach of this type was recently attempted in Ref. 25 in a weak-coupling regime. The applicability of such an approach is extremely limited at strong coupling, however.

The second option is to use a phenomenological expression for the Zeeman splitting as an input for the thermodynamic potential and minimize the latter only with respect to the gaps of interest. In *I* we used the latter approach, taking as an input the usual Zeeman splitting (3) and considering the thermodynamic potential with the singlet excitonic gap Δ in the weak-coupling regime with $g \simeq 0.07$.

The analysis is reliable in this regime, but the results do not describe all the features of the Hall conductivity in graphene quantitatively. In fact, the analysis of the data presented in Sec. II led us to the conclusion that the weak-coupling regime is most likely improbable. Therefore, here we insist on the strong-coupling regime to describe the physics of graphene. Our argument is the following. The singlet gap Δ in *I* was related to the Landau scale $L(B) = \sqrt{\hbar v_F^2 |eB|/c}$ via the solution of the gap equation, $\Delta = bL(B)$, where the dimensionless parameter b in the LLL approximation is given by

$$b = \frac{g}{\sqrt{2}} \int_0^\infty \frac{dk e^{-k^2}}{1 + k\chi_0}, \quad (15)$$

with $\chi_0 \simeq 0.56\sqrt{2}\pi g$. Since the estimate for the value of Δ obtained in Sec. II is by an order of magnitude larger than in *I*, the corresponding parameter $b = 0.4$ is also 10 times larger than in *I*. Then, using Eq. (15), we estimate that the value of the coupling constant is $g \sim 1.56$ which implies a strong-coupling regime.

In this regime, unfortunately, there exist no reliable schemes for treating the pairing dynamics quantitatively. As was emphasized in Ref. 29, the problem is due to non-decoupling of the low-energy dynamics on the LLL from the dynamics on higher Landau levels.

A general insight into the dynamics of magnetic catalysis at strong-coupling can be gained from the original work²⁷ in models with short range (contact) interactions in the leading order of $1/N$ expansion, where N is the

number of fermion ‘‘flavors’’ (N equals 2 in graphene). The dynamical picture following from that analysis is the following. While an external magnetic field strongly enhances the pairing dynamics, a nonzero density of carriers tends to suppress pairing. Moreover, for a wide range of parameters, the gap closes at the critical density that corresponds to filling the LLL. In terms of the chemical potential, this gives the critical value, $|\mu_c| = \Delta$ in the absence of the Zeeman splitting,²⁹ and $|\mu_c| = \Delta + E_Z$ when the Zeeman splitting is relevant.

In addition to the exciton condensation in graphene, one should also account for the anomalously large Zeeman splitting (11), which is likely to have a similar dynamical origin. As is discussed in *I* and in Sec. II above, it is the only way to remove completely the four-fold degeneracy of the lowest Landau level necessary for the explanation of the experimentally observed $\nu = 1$ plateau in the Hall conductivity.

Here, therefore, we implement all the details of the fermion pairing dynamics by making use of a simple phenomenological approach. In particular, we will use the simplest possible ansatz for the dynamically generated gaps Δ_\pm for the spin up and down states, which capture the essential features of the magnetic catalysis phenomenon discussed above. We write

$$\begin{aligned} \Delta_+(B, \mu) &= \Delta(B, \mu_+), \\ \Delta_-(B, \mu) &= \Delta(B, \mu_-), \end{aligned} \quad (16)$$

where, as already defined in the text after Eq. (2), $\mu_\pm = \mu \pm E_Z(B)$, with the Zeeman energy $E_Z(B)$ given in Eq. (11). Note that the triplet channel is taken into account by considering the two different gaps Δ_\pm corresponding to the order parameters $1/2\langle \bar{\Psi}(\sigma_0 \pm \sigma_3)\Psi \rangle$, respectively. The magnetic catalysis dynamics is mainly realized at the two Fermi surfaces, $\mu_\pm = 0$, connected with the spin up and down quasiparticles, and leads to the gaps of approximately the following form:

$$\Delta(B, \mu_\pm) = \frac{\Delta_0}{\pi} \theta(B - B_c) \sqrt{\frac{B}{B_c} - 1} \left[\arctan\left(\frac{\mu_\pm + \mu_c(B)}{\gamma}\right) - \arctan\left(\frac{\mu_\pm - \mu_c(B)}{\gamma}\right) \right]. \quad (17)$$

Here B_c is the critical field, γ is the LLL width (or quasiparticle scattering rate), and the dependence of the critical chemical potential on the field B is

$$\mu_c(B) = \Delta_0 \theta(B - B_c) \sqrt{\frac{B}{B_c} - 1}. \quad (18)$$

The expression (17) incorporates the following key features of the magnetic catalysis dynamics:

- (i) In view of expression (18), the gap is negligible for chemical potentials larger than the critical value

$\mu_c(B)$ which corresponds to the filling of the LLL, i.e., $\mu_c \simeq \Delta(B, \mu)|_{\mu=0}$ (see Ref. 27,29).

- (ii) In accordance with previous studies,²⁹ the magnetic catalysis occurs only when the field exceeds a critical value B_c .
- (iii) The effects due to non-vanishing scattering rate γ are incorporated through the smearing of the critical region around μ_c . Note that the choice of the arctan-function in the μ -dependence in Eq. (17) is

suggested by the $T = 0$ gap equation (A11) in *I*.

In total, we have three parameters, Δ_0 , B_c , and γ for the description of the gap generation, which can be used to fit the experimental data. In order to compare the theory and the experiment, we substitute the gaps Δ_{\pm} given in (16) [with $\Delta(B, \mu_{\pm})$ from Eq. (17)] and dependences $\mu(V_g)$ and $E_Z(B)$ in Eqs. (9) and (11) (extracted from the experimental data) into the expression for the

$$\tilde{\sigma}_{xy}(\Delta_{\pm}, \mu_{\pm}) = -\frac{2e^2 \text{sgn}(eB)}{\pi h} \text{Im} \left\{ \Psi \left(\frac{\gamma_{\text{tr}} + i(\mu_{\pm} + \Delta_{\pm})}{2\pi T} + \frac{1}{2} \right) - \frac{\gamma_{\text{tr}}}{2\pi T} \Psi' \left(\frac{\gamma_{\text{tr}} + i(\mu_{\pm} + \Delta_{\pm})}{2\pi T} + \frac{1}{2} \right) + (\Delta_{\pm} \rightarrow -\Delta_{\pm}) \right\}, \quad (20)$$

where γ_{tr} is the transport scattering rate. One can verify that for $T = \gamma_{\text{tr}} = 0$ and $\Delta_- = \Delta_+ = \Delta$, Eq. (19) reduces to Eq. (2).

IV. RESULTS AND THEIR INTERPRETATION

The best fit is obtained while using the following values of the parameters:

$$\Delta_0 = 680 \text{ K}, \quad (21a)$$

$$B_c = 7 \text{ T}, \quad (21b)$$

$$\gamma = \gamma_{\text{tr}} = 50 \text{ K}. \quad (21c)$$

Note that these parameters capture essentially all the non-perturbative physics of a strongly interacting model at hand. Remarkably, it is sufficient to get a nearly perfect fit for a wide range of the magnetic fields, see Fig. 4. In the upper panel of the Fig. 4, we present the experimental data for σ_{xy} , and in the lower panel their description within our phenomenological model.

The theoretical curves plotted in Fig. 4 at $T = 30$ mK remain practically the same over a very wide range of temperatures up to $T \lesssim \Delta_0$ when γ and γ_{tr} do not depend on T . At present there are no available experimental data for the temperature dependence of $\nu = 0, \pm 1$ and $\nu = \pm 4$ plateaus. Furthermore, to compare our model with such experimental data at high temperatures one should also take into account the dependence of γ and γ_{tr} on the temperature.

The large value of Δ_0 in Eq. (21a), which is necessary to fit the data, and the simple estimate of the coupling constant g made below Eq. (15) clearly imply a strong-coupling regime. The coupling constant is $g = e^2/\epsilon\hbar v_F = \alpha c/\epsilon v_F$, where $\alpha \simeq 1/137$ is the fine-structure constant. With air on one side of the graphene plane and SiO_2 on the other, the unscreened dielectric constant of the medium is estimated in Ref. 21 to be $\epsilon \approx 1.6\epsilon_0$. This corresponds to $g \approx 1.37$. We see that once again this supports the arguments that a strong-coupling regime

Hall conductivity:

$$\sigma_{xy} = \frac{1}{2} [\tilde{\sigma}_{xy}(\Delta_+, \mu_+) + \tilde{\sigma}_{xy}(\Delta_-, \mu_-)]. \quad (19)$$

The conductivity $\tilde{\sigma}_{xy}$ in the limit $B \rightarrow \infty$ can be expressed in terms of the digamma function $\Psi(x) = d \ln \Gamma(x)/dx$ (see Appendix B in *I*), namely

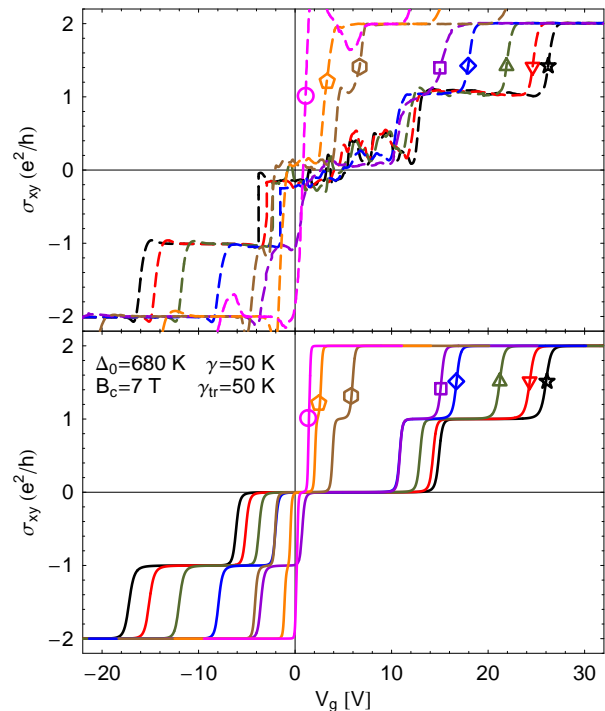


FIG. 4: (Color online) Hall conductivity from the data in Ref. 2 (upper panel) and in the theoretical model (lower panel) for magnetic fields $B = 9$ T (circle), 11.5 T (pentagon), 17.5 T (hexagon), 25 T (square), 30 T (diamond), 37 T (up triangle), 42 T (down triangle), and 45 T (star). The parameters in the model are $\gamma = \gamma_{\text{tr}} = 50$ K, and temperature $T = 30$ mK.

considered in this paper is more plausible than a weak-coupling one.

It is instructive to consider how the quasiparticle energy spectrum is affected by the applied gate voltage in graphene. Such a spectrum for a fixed value of the magnetic field is shown in Fig. 5. In essence, it is the

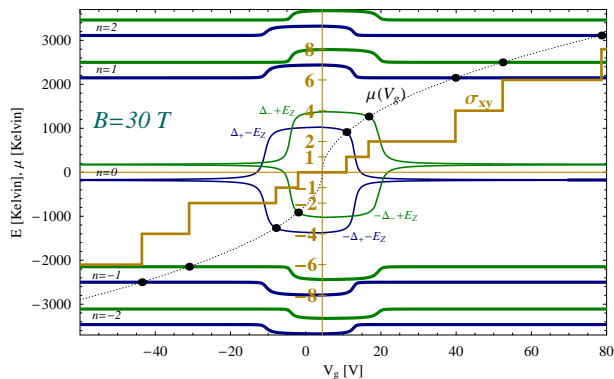


FIG. 5: (Color online) The theoretically reconstructed spectrum of one-particle excitations in graphene at a fixed value of the magnetic field, $B = 30$ T, as a function of the gate voltage. The energy levels are shown by solid lines of different thickness which represents the degeneracy of the Landau levels: thin and thick lines denote single and double degeneracy, respectively. The dotted line shows the dependence of the chemical potential on the gate voltage, see Eq. (9). The points of the intersection of the chemical potential with the energy levels marks the position of the steps between neighboring plateaus in the corresponding dependence of the Hall conductivity on the voltage.

strong-coupling pairing dynamics that is responsible for the drastic change of the energy spectrum at low voltage. The four-fold degeneracy of the LL level is lifted at low voltage because of the gap formation and the large Zeeman splitting. When the voltage (and, therefore, the chemical potential and the density) is large, the pairing plays no important role.

At large $|V_g|$, the LLL, which has the energy $E_0 = 0$ and the four-fold degeneracy in absence of Zeeman splitting, splits into two levels with the energies $E = \pm E_Z$ and with the two-fold degeneracy (thick lines), as shown in Fig. 5. When the absolute value of μ is such that $\mu_- = \mu - E_Z$ is smaller than the critical value $\mu_c(B)$, the gap Δ_- opens. This gap causes the level with $E = E_Z$ to split into two nondegenerate levels with energies $E = E_Z \pm \Delta_-$. Similar splitting of the energy level $E = -E_Z$ into two levels with energies $E = -E_Z \pm \Delta_+$ is caused by a nonzero Δ_+ when the value $\mu_+ = \mu + E_Z$ becomes smaller than $\mu_c(B)$. As should be clear from Fig. 5, it is only the presence of such nondegenerate levels in the energy spectrum of graphene that make the observation of the $\nu = \pm 1$ plateaus possible. In approximately the whole region where both gaps Δ_{\pm} are nonzero, the Hall conductivity of graphene develops the $\nu = 0$ plateau. Moreover, this correspondence might be exact if the phase transition with respect to V_g (or μ) is a strong first order phase transition.

It should be noted that the mechanism behind the creation of the $\nu = 0, \pm 1$ plateaus in the strong-coupling regime is different from that at weak coupling. In the latter case, the dominant term responsible for the creation

of the $\nu = 0$ for small μ (or $V_g \sim V_0$) is the excitonic gap Δ , while the $\nu = \pm 1$ plateaus are related to the Zeeman term (see the discussion after Eq. (12) above and Fig. 1 in *I*). In the present scenario with a strong-coupling dynamics, there are two gaps, Δ_{\pm} , and for $T = \gamma_{tr} = 0$ Eq. (19) reduces to

$$\sigma_{xy} = -\frac{e^2}{h} \text{sgn}(eB) \times [\text{sgn}(\mu_+) \theta(|\mu_+| - \Delta_+) + \text{sgn}(\mu_-) \theta(|\mu_-| - \Delta_-)] \quad (22)$$

instead of a more simple Eq. (2). For the case $E_Z < \Delta_{\pm}$ shown in Fig. 5, this dependence of σ_{xy} on μ implies that while the size of the 0th plateau is $\delta\mu_0 = |\Delta_+ + \Delta_- - 2E_Z|$, the size of the ± 1 plateaus is $\delta\mu_{\pm 1} = |\Delta_- - \Delta_+ + 2E_Z|$. When the effects of non-vanishing widths γ and γ_{tr} are taken into account, the results become more complicated of course. However, the main qualitative features regarding the $\nu = 0, \pm 1$ plateaus are captured already by Eq. (22). It is clear, for example, that these plateaus result from a subtle interplay between the gaps Δ_{\pm} and the Zeeman energy. We also note that the $\nu = \pm 1$ plateaus disappear when $\Delta_{\pm} = 0$. It is also absent when $E_Z = 0$ and $\Delta_+ = \Delta_-$ (see also the next section).

V. HALL CONDUCTIVITY WITHOUT ENHANCED ZEEMAN SPLITTING

In order to appreciate the role of the enhanced Zeeman splitting, which is required to fit the data in Ref. 2, it will be instructive to consider also the case without Zeeman splitting, i.e., $E_Z = 0$. It should be clear that this approximation should also describe well a system with an unenhanced Zeeman energy E_Z , as given in Eq. (3), when $E_Z \lesssim \gamma$. By making use of the same model parameters as in the previous section, see Eq. (21), we plot the theoretical curve for the Hall conductivity as a function of the gate voltage in Fig. 6.

To calculate the dependence of the Hall conductivity on the gate voltage, here we used the expressions in Eqs. (3.14) and (3.15) in Ref. 14. The corresponding result includes the contributions of all Landau levels, which are needed in order to reproduce not only the lowest plateaus with $|\nu| \leq 2$, as in Fig. 4, but also the higher ones.

As we see from Fig. 6, the plateaus with $\nu = \pm 1$ and $\nu = \pm 4k$ (with integer k) do not appear when the Zeeman energy is negligible (or $E_Z \lesssim \gamma$). Of course, this conclusion is hardly surprising in view of the correspondence between the energy spectrum in graphene and the form of the Hall conductivity illustrated in Fig. 5. When the Zeeman splitting of the Landau levels disappears, the plateaus with $\nu = \pm 1, \nu = \pm 4, \nu = \pm 8$, etc. collapse into a point. In the language of symmetry, this picture corresponds to a partial removing the degeneracy of the LLL, when the $U(4)$ symmetry is broken down to the $U(2)_a \times U(2)_b$ (see Appendix C in *I*).

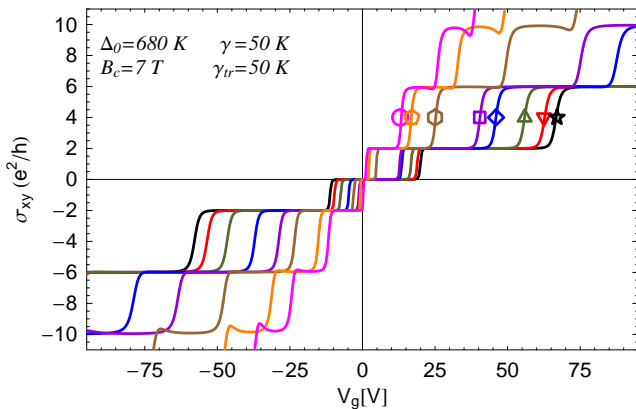


FIG. 6: (Color online) Hall conductivity in the case of a negligible Zeeman energy. As in Fig. 4, the symbols label different values of the magnetic field: $B = 9$ T (circle), 11.5 T (pentagon), 17.5 T (hexagon), 25 T (square), 30 T (diamond), 37 T (up triangle), 42 T (down triangle), and 45 T (star).

VI. CONCLUSION

In this paper, based on the experimental data of Ref. 2, we developed a model for the exciton condensation dynamics in graphene in a strong magnetic field. The non-perturbative dynamics corresponds to a strong coupling regime with a realistic value of the coupling constant $g = e^2/\epsilon\hbar v_F$ of the Coulomb interaction.

On theoretical side, the model incorporates the main features of the phenomenon of the magnetic catalysis²⁷ (the generation of an excitonic gap in a strong magnetic field) and its realization in graphene considered in Refs. 28,29. On phenomenological side, the model is based on features extracted from the experimental data in Ref. 2. Among them, the relation between the gate voltage applied to the graphene device and the chemical potential μ is particularly important. Another important point established is a strong enhancement of the Zeeman splitting (spin gap) in graphene in strong magnetic fields $B \gtrsim 9$ T. The existing experimental data, however, do not allow to extract the dependence of the spin gap on T and μ and here we considered its dependence on the field B only.

The enhanced Zeeman splitting alone does not allow to explain the occurrence of the additional plateaus with the filling factors $\nu = \pm 1$ in magnetic fields $B \gtrsim 20$ T observed in Ref. 2. In addition to such a splitting, it is necessary to remove the sublattice degeneracy in graphene to explain the origin of these plateaus. The available experimental data² already contain a lot of constraints on possible microscopical mechanism which removes this degeneracy. In addition to this, the observation of the $\nu = 0$ plateau at rather high temperatures³ indicates that a strong coupling regime is more believable than the weak coupling regime.

Still further experiments are necessary to establish the temperature evolution of the $\nu = 0, \pm 1, \pm 4$ plateaus and their sensitivity to the quality of the samples. This will hopefully allow to decide which of the mechanisms mentioned in the Introduction is realized in graphene in a strong magnetic field. For example, there is a suggestion how to detect a gap either in microwave³⁶ or optical³⁷ response. Recent measurements done in the far infrared region^{38,39} show that the second method may work if the measurements will be done not in epitaxial graphite as in Ref. 38 or in highly oriented pyrolytic graphite as in Ref. 39 but in graphene in a strong magnetic field.

Acknowledgments

We are grateful to P. Kim and Y. Zhang for sending us original experimental data of their work² and to A.K. Geim for discussing with us the unpublished results. Useful discussions with J.P. Carbotte are acknowledged. The work of V.P.G. was supported by the SCOPES-project IB7320-110848 of the Swiss NSF and by Ukrainian State Foundation for Fundamental Research. The work of V.A.M. was supported by the Natural Sciences and Engineering Research Council of Canada. He acknowledges the warm hospitality of Prof. Taichiro Kugo and Prof. Teiji Kunihiro during his stay at Yukawa Institute for Theoretical Physics. The work of S.G.S. was supported by the Natural Sciences and Engineering Research Council of Canada and the Canadian Institute for Advanced Research.

* On leave from Bogolyubov Institute for Theoretical Physics, 03143, Kiev, Ukraine

¹ V.P. Gusynin, V.A. Miransky, S.G. Sharapov, and I.A. Shovkovy, Phys. Rev. B **74**, 195429 (2006).

² Y. Zhang, Z. Jiang, J.P. Small, M.S. Purewal, Y.-W. Tan, M. Fazlollahi, J.D. Chudow, J.A. Jaszczak, H.L. Stormer, and P. Kim, Phys. Rev. Lett. **96**, 136806 (2006).

³ A.K. Geim, private communication.

⁴ K.S. Novoselov, A.K. Geim, S.V. Morozov, D. Jiang, Y. Zhang, S.V. Dubonos, I.V. Grigorieva, and A.A. Firsov,

Science **306**, 666 (2004).

⁵ A.K. Geim and K.S. Novoselov, Nature Mat. (2007) (unpublished).

⁶ A.H. Castro Neto, F. Guinea, and N.M. Peres, Physics World **19**, 33 November (2006).

⁷ G.W. Semenoff, Phys. Rev. Lett. **53**, 2449 (1984).

⁸ D.P. DiVincenzo and E.J. Mele, Phys. Rev. B **29**, 1685 (1984).

⁹ G.P. Mikitik and Yu.V. Sharlai, Phys. Rev. Lett. **82**, 2147 (1999).

- ¹⁰ S.G. Sharapov, V.P. Gusynin, and H. Beck, Phys. Rev. B **69**, 075104 (2004).
- ¹¹ V.P. Gusynin and S.G. Sharapov, Phys. Rev. B **71**, 125124 (2005).
- ¹² Y. Zheng and T. Ando, Phys. Rev. B **65**, 245420 (2002).
- ¹³ V.P. Gusynin and S.G. Sharapov, Phys. Rev. Lett. **95**, 146801 (2005).
- ¹⁴ V.P. Gusynin and S.G. Sharapov, Phys. Rev. B **73**, 245411 (2006).
- ¹⁵ N.M.R. Peres, F. Guinea, and A.H. Castro Neto, Phys. Rev. B **73**, 125411 (2006).
- ¹⁶ K.S. Novoselov, A.K. Geim, S.V. Morozov, D. Jiang, M.I. Katsnelson, I.V. Grigorieva, S.V. Dubonos, and A.A. Firsov, Nature **438**, 197 (2005).
- ¹⁷ Y. Zhang, Y.-W. Tan, H.L. Störmer, and P. Kim, Nature **438**, 201 (2005).
- ¹⁸ V.M. Apalkov, T. Chakraborty, Phys. Rev. Lett. **97**, 126801 (2006).
- ¹⁹ C. Toke, P.E. Lammert, J.K. Jain, and V.H. Crespi, Phys. Rev. B **74**, 235417 (2006).
- ²⁰ D.V. Khveshchenko, cond-mat/0607174.
- ²¹ J. Alicea and M.P.A. Fisher, Phys. Rev. B **74**, 075422 (2006).
- ²² In the both cases, the $SU(4)$ is associated with spin-pseudospin degrees of freedom, but while in graphene pseudospin is related to the sublattice index, in bilayer quantum Hall systems pseudospin is related to the layer index.
- ²³ K. Nomura and A. H. MacDonald, Phys. Rev. Lett. **96**, 256602 (2006).
- ²⁴ M.O. Goerbig, R. Moessner, and B. Douçot, Phys. Rev. B **74**, 161407(R) (2006).
- ²⁵ I.F. Herbut, Phys. Rev. Lett. **97**, 146401 (2006); cond-mat/0610349.
- ²⁶ M. Ezawa, cond-mat/0609612.
- ²⁷ V.P. Gusynin, V.A. Miransky, and I.A. Shovkovy, Phys. Rev. Lett. **73**, 3499 (1994); Phys. Rev. D **52**, 4718 (1995); Nucl. Phys. B **462**, 249 (1996).
- ²⁸ D.V. Khveshchenko, Phys. Rev. Lett. **87**, 206401 (2001); *ibid.* **87**, 246802 (2001).
- ²⁹ E.V. Gorbar, V.P. Gusynin, V.A. Miransky, and I.A. Shovkovy, Phys. Rev. B **66**, 045108 (2002).
- ³⁰ E.V. Gorbar, V.P. Gusynin, V.A. Miransky, and I.A. Shovkovy, Phys. Lett. A **313**, 472 (2003).
- ³¹ H. Leal and D.V. Khveshchenko, Nucl. Phys. B **687**, 323 (2004); D.V. Khveshchenko and W.F. Shively, Phys. Rev. B **73**, 115104 (2006).
- ³² Y. Kopelevich, V. V. Lemanov, S. Moehlecke, and J. H. S. Torres, Fiz. Tverd. Tela **41**, 2135 (1999) [Phys. Solid State **41**, 1959 (1999)]; H. Kempa, Y. Kopelevich, F. Mrowka, A. Setzer, J. H. S. Torres, R. Höhne, and P. Esquinazi, Solid State Commun. **115**, 539 (2000); M. S. Sercheli, Y. Kopelevich, R. R. da Silva, J. H. S. Torres, and C. Rettori, Solid State Commun. **121**, 579 (2002). For the latest results of this group, see Y. Kopelevich, J. C. Medina Pantoja, R. R. da Silva, F. Mrowka, and P. Esquinazi, Phys. Lett. A **355**, 233 (2006).
- ³³ J.-N. Fuchs and P. Lederer, cond-mat/0607480, to appear in Phys. Rev. Lett.
- ³⁴ D.A. Abanin, P.A. Lee, and L.S. Levitov, Phys. Rev. Lett. **96**, 176803 (2006).
- ³⁵ Note that in contrast to the Zeeman term $\overline{\Psi}\gamma^0\sigma_3\Psi$, which is proportional to the difference of the total densities of the spin up and down components, the triplet excitonic gap term $\overline{\Psi}\sigma_3\Psi$ in Eq. (14) is related to the electron spin density imbalance between the A and B sublattices of the bipartite hexagonal lattice of the graphene sheet.^{28,31} As is clear from Eq. (13), the singlet excitonic gap term $\overline{\Psi}\sigma_0\Psi$ is the electron charge density imbalance between the A and B sublattices. In Ref. 25, the corresponding order parameters are called the antiferromagnetic and charge-density waves, respectively.
- ³⁶ V.P. Gusynin, S.G. Sharapov and J.P. Carbotte, Phys. Rev. Lett. **96**, 256802 (2006).
- ³⁷ V.P. Gusynin, S.G. Sharapov and J.P. Carbotte, cond-mat/0607727.
- ³⁸ M.L. Sadowski, G. Martinez, M. Potemski, C. Berger, and W.A. de Heer, cond-mat/0605739, to appear in Phys. Rev. Lett.
- ³⁹ Z. Q. Li, S.-W. Tsai, W. J. Padilla, S. V. Dordevic, K. S. Burch, Y. J. Wang, and D. N. Basov, Phys. Rev. B **74**, 195404 (2006).